ON THE CONSTRUCTAL OPTIMAL SHAPE OF MAGNETIC FIELD SOURCE USED IN MAGNETIC DRUG TARGETING

Alina M. SĂNDOIU[1], Alexandru M. MOREGA[2,3], Mihaela MOREGA[2]

Magnetic drug targeting (*MDT*) *is a medical procedure under current research, aimed to be a complementary technique for cancer treatment. In MDT, the drug molecules are carried by super-paramagnetic particles and delivered to targeted areas through blood flow under the action of a magnetic field. The magnetic field source considered here for MDT is a permanent magnet and this paper is about its optimization, with the aim to obtain high magnetic body forces, which may enhance the MDT effect.*

Keywords: magnetic drug targeting, constructal law, optimization, permanent magnet, numerical simulation

1. Introduction

The common treatment method for cancerous tumors, the chemotherapy, can be administrated either oral, or intravenous but the effects of the medication affects the whole body, even the healthy cells. The most important side effects of this procedure are infections, anemia, fever, and hair loss [1]. On the other hand, *magnetic drug targeting* (MDT) is a noninvasive procedure aimed to guide and fix the drugs in the target volume, to more efficiently treat the malignant tumors [2–5] while minimizing the mentioned side effects. It consists of drug carrying super–paramagnetic particles that are guided to the targeted area under the action of an external magnetic field.

Super–paramagnetic nanoparticles are widely used as carriers in biomedical applications such as magnetic resonance imaging and hyperthermia treatment [6]. The medication is delivered to the affected area using guidance under magnetic resonance imaging, ultrasound, or computer tomography. The mostly used nanoparticles with superparamagnetic properties in biomedical applications are SPIONs (superparamagnetic iron oxide nanoparticles), with iron oxide content.

[1] Dept. of Bioengineering an Biotechnology, Faculty of Medical Engineering, Doctoral School of Electrical Engineering, University POLITEHNICA of Bucharest, Romania, e-mail: alina.sandoiu@gmail.com

[2] Laboratory of Electrical Engineering in Medicine, Faculty of Electrical Engineering, University POLITEHNICA of Bucharest, Romania, e-mail: amm@iem.pub.ro, mihaela@iem.pub.ro

[3] "Gheorghe Mihoc – Caius Iacob" Institute of Mathematical Statistic and Applied Mathematics, Romanian Academy

They are made of particles of magnetite (Fe_3O_4) or magmatite ($y–Fe_2O_3$), and coated with organic or anorganic biocompatible polymers. Should the size of the nanoparticle be less than 30 nm, they lose their remanent magnetization to become super–paramagnetic. In intense magnetic fields, the magnetic moments of the particles align themselves in the direction of the field [6].

SPIONs are introduced in the venous stream to be naturally conveyed by the arterial flow near the region of interest, ROI. With the help of localized magnetization forces, they cross the vessel walls and the adjacent embedding tissue into the ROI. MDT can be used to guide and control the motion of SPIONs and acts as a complementary intervention for standard chemotherapy; its most important advantage is to reduce the aggressive side effects [7].

This paper is about the *constructal optimization* [8] of the permanent magnet, which is the commonly used magnetic field source, in order to generate high magnetic body forces aimed to enhance the targeting effect of the magnetic field – "shape with a purpose". The magnet here is a parallelepipedical, uniformly magnetized bar. Different design configurations and optimization criteria are possible of which we single out the design optimization strategy where the magnet may be split into several smaller, identical, parallelepipedical magnetic bars (called "slots"), with the aim to optimally cover a ROI. The size of slot edge along the split direction (the *slot width*, SW) and the spacing between the slots (the *gap size*, GS) are the optimization parameters. The total volume of the magnetic material is invariant.

First, a simpler 2D analysis is staged, and the magnetic forces acting on the magnetic medication are evaluated and optimal design criteria for the magnet are discussed. The blood aggregate fluid including the magnetic nanoparticles is further called magnetizable aggregate fluid (MAF). The magnetic field and the pending magnetic body forces are calculated then for different magnetic slot–arrays. Next, a similar 3D analysis is conducted, and its results are compared with those produced by the 2D study. Finally, the MAF flows are modeled for two optimized magnetic field sources.

2. The mathematical model for the MDT

The computational domain represents a simplified adult upper arm, and it comprises a larger blood vessel (*e.g.*, a vein, as the medication is delivered intravenously), the *humerus*, the muscular mass, the adjacent tissues, and a certain volume of air needed to conveniently close the magnetic field. The magnetic field produced by the permanent magnet is static, described by [8,9]

$$\text{Constitutive law} \qquad \begin{aligned} \mathbf{B} &= \mu_0 \mu_{r,mag} \mathbf{H} + \mathbf{B}_{rem} \quad (\text{permanent magnet}), \\ \mathbf{B} &= \mu_0 \mu_{r,ff} \mathbf{H} \quad (\text{agregate fulid}), \\ \mathbf{B} &= \mu_0 \mathbf{H} \quad (\text{elsewhere}), \end{aligned} \tag{1}$$

Ampère's law $$\nabla \times \mathbf{H} = 0, \tag{2}$$

Magnetic flux law $$\nabla \cdot \mathbf{B} = 0, \tag{3}$$

Here μ_0 [H/m] is the magnetic permeability of free space, $\mu_{r,mag}$ the relative permeability of the permanent magnet, $\mu_{r,ff}$ the relative permeability of the MAF, **H** [A/m] the magnetic field strength, **B** [T] the magnetic flux density, and $\mathbf{B}_{rm}$ the remanent flux density of the permanent magnet.

In virtue of eq. (1), the magnetic scalar potential V_m [A] may be used, $\mathbf{H} = -\nabla V_m$, yielding the following mathematical model for eqs. (1) – (3)

$$\nabla \cdot \left(\mu_0 \mu_r \nabla V_m + \mathbf{B}_{rm}\right) = 0, \tag{4}$$

where $\mu_r = \left\{\mu_{r,mag}, \mu_{r,ff}, 1\right\}$ for the magnet, MAF, and elsewhere, respectively. All magnetic media are assumed linear, homogeneous, and isotropic.

The boundary condition that closes the problem is magnetic insulation, *i.e.*, $\partial V_m / \partial n = 0$ where **n** is the outward pointing normal to the boundary.

We assume that the MAF is Newtonian and the hemodynamic flow is stationary, laminar, incompressible, described by [8]

Momentum balance (*Navier–Stokes*)

$$\rho(\mathbf{u} \cdot \nabla)\mathbf{u} = \nabla\left[-p\mathbf{I} + \eta\left((\nabla \mathbf{u}) + (\nabla \mathbf{u})^T\right)\right] + \mathbf{f}_{mg}, \tag{5}$$

Mass conservation

$$\nabla \cdot \mathbf{u} = 0, \tag{6}$$

where p [Pa] is the pressure, **I** unity matrix, **u** [m/s] the velocity field, ρ [kg/m^3] mass density, η [Pa·s] dynamic viscosity of MAF. Here ρ = 1000 kg/m^3 and η = 3.5 mPa·s. The magnetic body forces, $\mathbf{f}_{mg}$ [N/m^3], may be calculated using as the gradient of the magnetic energy density, $\mathbf{f}_{mg} = \nabla(\mathbf{B} \cdot \mathbf{H})/2$, [5].

The boundary conditions are as follows: uniform inlet velocity profile (U_{in} = 0.17 m/s [10]), uniform (zero) outlet pressure, and no–slip at the vessel walls.

A one–way coupling is assumed between the magnetic field and flow problems: the magnetic field (through the magnetization body forces) may influence the flow while the MAF flow does not perturb the magnetic field. The mathematical model is solved numerically using the finite element method (FEM) for the 2D models, and the boundary element method, for the 3D models [11]. Quadratic Lagrange elements are used to resolve magnetic field. For the flow part of the model, as there is no convection–diffusion associated problem (here, the magnetic field is independent of the flow), the default P1+P1 model is adequate (the velocity and the pressure are resolved with the same, 1st order, linear computational elements). The solver is conjugate gradients with left preconditioning, and algebraic multigrid (5 levels).

3. Numerical simulation results and discussion

Bidimensional (cartesian), Fig. 1 (for the magnetic field), and 3D models, Fig. 5 and Fig. 10 (magnetic field and flow), were utilized. The computational domains contain a vessel segment filled with MAF, the permanent magnet, and the surrounding nonmagnetic media (biological tissue, bone mass, and air above the skin). In this the 2D cartesian approach, it is understood that the 2D model is representative for the 3D case. It follows that the per meter quantities (*e.g.*, forces per unit length [N/m]) may be extrapolated, in an order of magnitude sense to their 3D counterparts (*i.e.*, forces [N]) by multiplying them with an equivalent "depth" of the 2D model. We use here the radius of the blood vessel, presented later in this paper, set to d = 6 mm. For a 6 mm thick magnet of V = 1.2 cm volume^3, which may cover the artery, the area of the bidimensional representation is 0.2 cm^2.

The volume size is an optimization constraint. The magnetic field problem (4) is solved for, with the aim to evaluate the magnetic body forces in the MAF, and find the optimal *aspect ratio of the permanent magnet*, A (A = height over width). The permanent magnet has $\mathbf{B}_{rm} = B_{rm}\mathbf{j}$, where B_{rm} = 1.3 T (*e.g.*, N50NdFeB N42, N45, N48 [12], or SmCo magnets [13]), and **j** is the unit vector in *Oy* direction (Fig. 1). By reasons of symmetry, a reduced computational domain was used, Fig. 1. Next, the permanent magnet is split into several identical, equally spaced parts ("slots"), in order to maximize the magnetic body force (the objective) within the MAF. The number of slots, NS, the slot width, SW = 7…10 mm, and the spacing between them, GS = 1…6 mm are optimization parameters. The magnet could be split into two, three, etc. slots, a sequence of arrays that points out a limit of consistency – for increasing NS and GS, the slots act more and more as independent magnets.

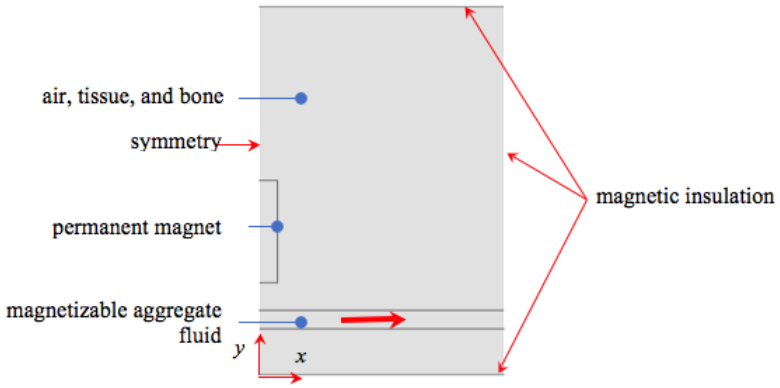

Fig. 1. The 2D computational domain and the magnetic field boundary conditions

Figure 2 shows bell–shaped curves for $F^*_{mg,x}$ (*Ox* component, stream–wise) and $F^*_{mg,y}$ (*Oy* component, orthogonal to the flow) when A is the degree of freedom

(optimization parameter). Here $F^*_{mg(x|y)} = d\int_{S_w} f_{mg(x|y)}\,\mathrm{d}x$ where S_w is the cross–sectional area of the MAF volume. Both forces, $F^*_{mg,x}$ and $F^*_{mg,y}$, show off maxima, of different magnitudes, for different values of A.

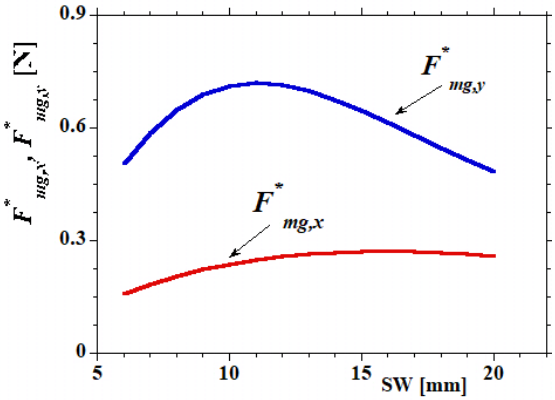

Fig. 2. The magnetic body forces for the undivided magnet – 2D analysis

Apparently, $F^*_{mg,y}$ acts into either attracting the medication towards the magnet, for $y > 0$, or repelling the medication, for $y < 0$. On the other hand, $F^*_{mg,x}$ contributes to mixing the MAF: for $x > 0$ it is opposite to the flow, and for $x < 0$ it accelerates the flow. Here, $x = 0$ corresponds to the position of the symmetry axis of the magnet. The magnet should be positioned such that the tumoral volume is located between the magnet and the blood vessel that caries the medication, and that the mixing effect is more significant during the low flow rate interval, for pulsating flow.

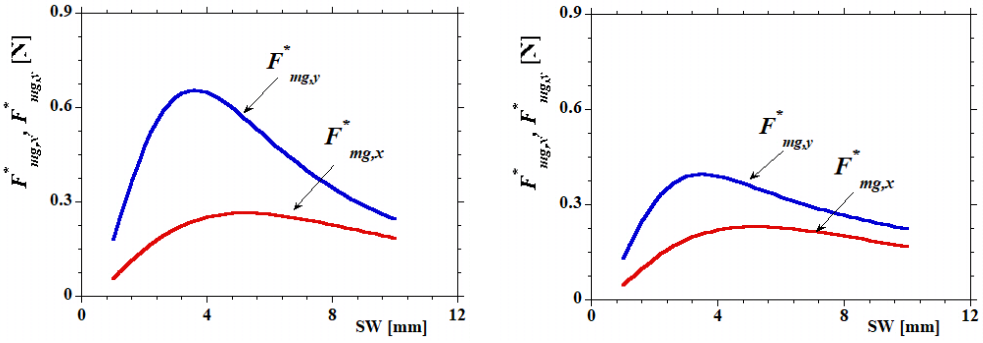

GS = 1 mm GS = 6 mm

Fig. 3. The magnetic body forces for an array of NS = 3 slots – 2D analysis

Figure 3 shows $F^*_{mg,x}$ and $F^*_{mg,y}$ *vs.* SW when the magnet is divided into NS = 3 identical, equally spaced slots, for two limiting values, GS = 1 mm and GS = 6 mm.

SW, instead of A, is now the second design parameter. Designs with GS > 6 mm may result in quasi–independent, non–interacting magnets. The maxima of $F^*_{mg,x}$ and $F^*_{mg,y}$ decrease with GS (by half from 6 mm to 1 mm), and they occur for (almost) the same values of GS. We may conclude that GS = 1 mm (the smallest GS) provides for an optimum. The optimal configuration of the magnet was found in the interval SW = 3…4 mm. Depending on the morphology of the targeted tumoral volume, the therapist may decide the optimal configuration for the magnet (GS and SW of the array of magnetic slots) for a specific ROI morphology. The same analysis (GS and SW optimization) was performed for the magnet split into NS = 4,5,6 slots. For instance, for NS = 5, the maximum value for $F^*_{mg,y}$ occurs for a thinner (slender) slot (SW = 0.002 mm) when comparing to the NS = 3. Figure 4 exemplifies $F^*_{mg,x}$ and $F^*_{mg,y}$, for GS = 1 mm and GS = 6 mm, when NS = 5.

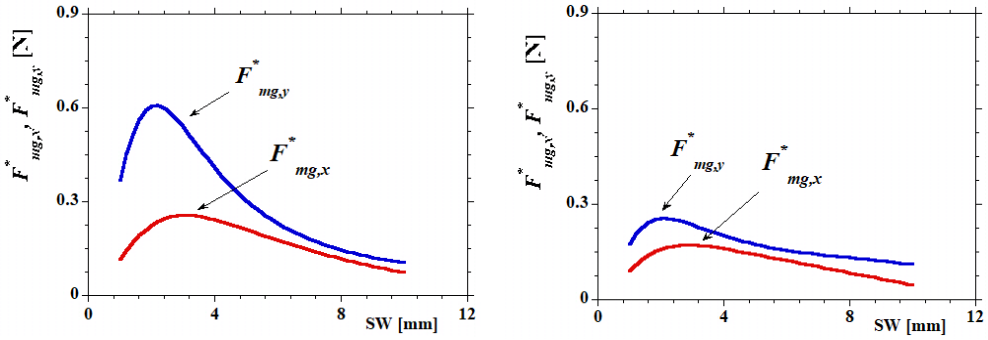

GS = 1 mm GS = 6 mm

Fig. 4. The magnetic body forces for an array of NS = 5 slots – 2D analysis

A more realistic geometry was used in the 3D analysis, Fig. 5.

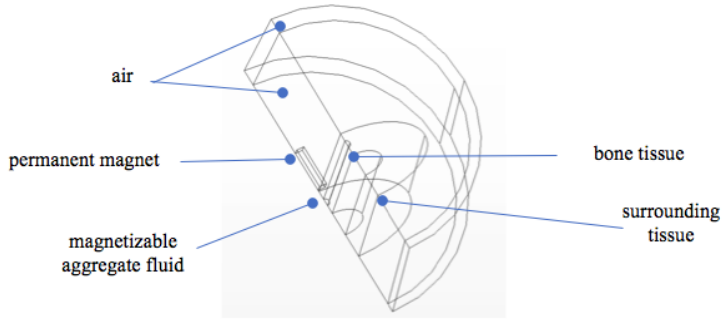

Fig. 5. The reduced 3D computational domain in the magnetic field problem.

"Infinite" elements [6] are used to border the computational domain and close the magnetic field at a finite distance, and symmetry is used, leading to a

substantial reduction in mesh size. An unstructured discretization (Delaunay) mesh with *approx.* 540.000 tetrahedral elements is used to provide for grid independent numerical solutions. Figure 6 presents the components of the total magnetic force for the unsplit magnet. Apparently, the streamwise, $F_{mg,z}$, and normal to flow, $F_{mg,y}$, components occur for the (almost) same value of GS, whereas the $F_{mg,x}$ (lateral) component is recorded for a (slightly) smaller GS.

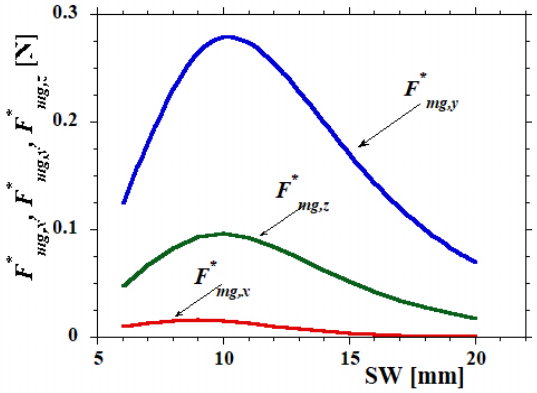

Fig. 6. The magnetic force for the unsplit magnet – 3D analysis

Table 1 summarizes optimization results for the magnet split into NS = 3,4,5 identical slots. The GS limiting sizes only are reported here. SW, related to GS, is the running the optimization parameter.

Table 1

Magnetization forces maxima recorded along the top most streamline inside the blood vessel and the corresponding magnet design parameters for different magnet configurations

NS [–]	GS [mm]	SW_{opt} [mm]	$F_{mg,x}$ [N]	SW_{opt} [mm]	$F_{mg,y}$ [N]	SW_{opt} [mm]	$F_{mg,z}$ [N]
3	1	7.4	0.019051	8.6	0.272633	8	0.07751
	6	7.6	0.012235	8.8	0.181689	8.4	0.038709
4	1	8.8	0.015457	10	0.262231	9.8	0.087083
	6	8.8	0.011722	10	0.198195	9.2	0.04515
5	1	6.2	0.02113	7	0.2621	6.2	0.056329
	6	6.4	0.011493	7.4	0.157431	6.8	0.020921

For NS = 3, $F_{mg,z}$ may play a role if it is to cover a larger surface of the artery. The $F_{mg,x}$ component extracts part of the medication out of the blood vessel, into the tissue. The results are consistent with the 2D ones, and the maxima of the force components decrease when GS increases. However, the 3D values are smaller, but of the same order of magnitude, than their 2D counterparts. The reason is that the extrapolated 2D MAF volume is almost half the 3D MAF one, while the average magnetic flux field tube length is shorter. Hence, the 2D model produced a more

intense field than the 3D one. Moreover, the magnetic energy in the 3D magnet enables also the $F_{mg,x}$ force component. Also the maxima shift w.r.t. SW is less apparent. The magnetic force transversal to the flow, $F_{mg,x}$, does not exist in the 2D model. The optimal design, with the highest magnetic forces, may correspond to GS = 1 mm.

For NS = 4 too the maxima decrease when GS increases, however they are lower than those obtained for NS = 3. The magnetic forces are smaller if GS is larger, *e.g.*, a lower value for $F_{mg,z}$ is recorded for GS = 6 mm. However a larger area of the blood vessel is covered. This aspect may suggest a tradeoff optimal design solution – a large enough force over a large enough area. To render the bell shape of the magnetic forces distribution, Fig. 7 compiles the results for NS = 5.

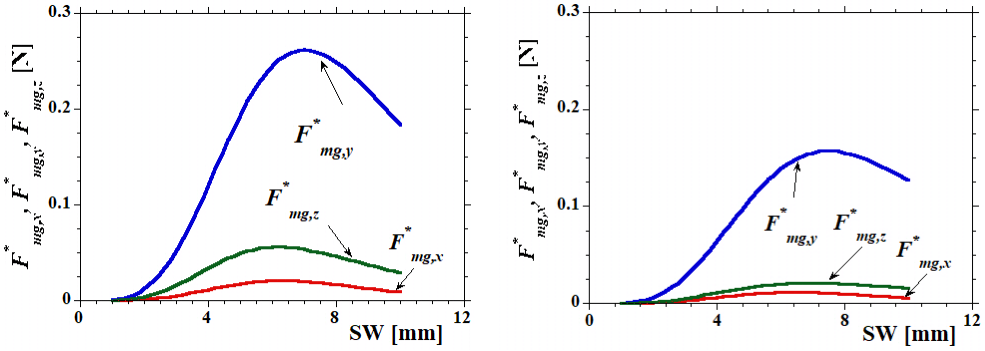

GS = 1 mm GS = 6 mm

Fig. 7. The magnetic forces for an array of NS = 5 slots – 3D analysis

Finally, we consider the MAF flow under the influence of the magnetic field.

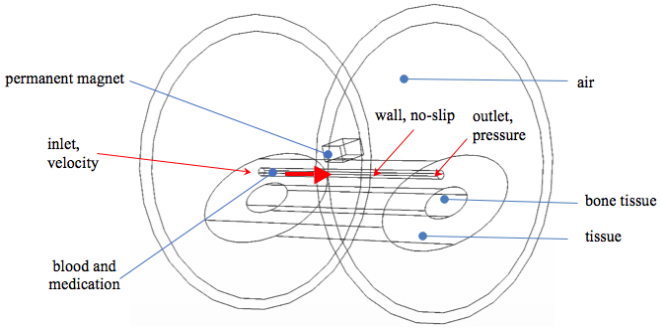

Fig. 8. The 3D computational domain and the boundary conditions in the hemodynamic problem

Figure 8 shows the computational domain and the boundary conditions for the hemodynamic problem (the blood vessel only). Two, twice optimized (GS and SW) magnetic source configurations, are shown here, NS = 1 and 5. The magnetic body forces are significant between the magnet and the MFA volume (Fig. 9).

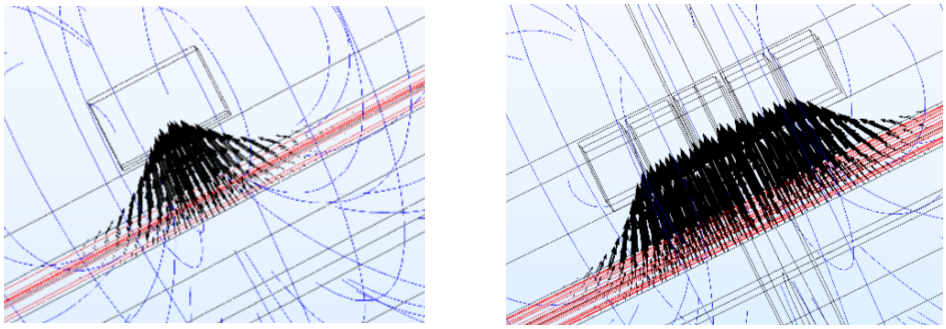

a. The unsplit magnet, NS = 1 slot b. The array of magnets with NS = 5 slots

Fig. 9. Magnetic flux density (blue lines), velocity (red lines), and magnetic body forces (arrows)

Table 2 lists $F_{mg,y}$ maxima. Here AL is the linear size of magnetic array in streamwise direction, computed as $AL = NS \times SW + (NS-1) * GS$. Apparently, the array with NS = 2 slots provides for the best specific extraction force.

Table 2

The total force that different configurations of the magnetic field source

Number of slots, NS	1	2	3	5
$F_{mg,y}$ [N]	1.0763	1.0632	1.0512	1.0093
$F_{mg,y}/(AL \times SW)$ [N/m²]	5381.5	5483.23	4684.49	3697.07

The total force acting in the flow direction upon the MAF is $F_{total} = \int_S p\,\mathrm{d}S + \int_V F_{mg,z}\,\mathrm{d}V$, where S is cross sectional area of the vessel, and V is the volume of the MAF. The magnetic term contributes to the mixing of the MAF.

4. Conclusions

This paper is about the constructal optimization of the MDT permanent magnet with the aim to maximize the targeting effect of the magnetic field – "shape with a purpose". The design optimization strategy concerns the magnet spliting into several smaller, identical, parallelepipedical magnetic bars (called "slots"). The total volume of the magnetic material is kept invariant, while the size of slot edge along the split direction (the *slot width*, SW) and the spacing between the slots (the *gap size*, GS) are two other optimization parameters.

The maxima for the streamwise (with mixing effect) and $\mathbf{B}_{rm}$–oriented (with medication extraction effect) components of the total magnetic force in 2D model are consistent with the 3D results, but different shifting with respect to SW for the $\mathbf{B}_{rm}$–oriented (extraction) force was found.

Magnet splitting leads to the decrease of the total extraction force. However its specific (per surface unit) counterpart, obtained by dividing the total force to the area of the planar footprint of the magnetic array, exhibits a maximum. This results

points out a trade–off optimization solution: a large enough extraction force for a large enough surface to be covered. The magnet ought to be placed such that the tumoral ROI is between the magnet and the blood vessel that delivers the medication. Based on the size, morphology and position of the tumor, the therapist can decide the optimal design for the magnet (NS, GS, and SW) to be utilized. More accurate result can be obtained on patient–related realistic models constructed by using medical images reconstruction techniques rather than CAD – the subject of a further study.

ACKNOWLEDGEMENTS

The works was conducted in the Laboratory for Electrical Engineering in Medicine, affiliated with BIOINGTEH, at the University POLITEHNICA of Bucharest. The first author acknowledges the support granted by the project POSDRU 134398.

R E F E R E N C E S

[1]. *A.S. Lubbe, et al.,* "Clinical experiences with magnetic drug targeting: A phase I study with 4'–epidoxorubicin in 14 patients with advanced solid tumors", Cancer Res., **vol. 56**, no. 20, pp. 4686–4693, 1996.
[2]. *N.M, Orekhova, R.S. Akchurin, A.A. Belyaev, M.D. Smirnov, S.E. Ragimov, A.N. Orekhov*, "Local prevention of thrombosis in animal arteries by means of magnetic targeting of aspirin–loaded red cells", Thrombosis Res., **vol. 57**, pp. 611–616, 1990.
[3]. *A. Nacev, C. Beni, O. Bruno, B. Shapiro*, "The behaviors of ferro–magnetic nano–particles in and around blood vessels under applied magnetic fields", J. Magn. Magn. Mater. 2011, **vol. 323**, 6, pp. 651–668, March 1, 2011.
[4]. *A. Drochon, V. Robin, O. Fokapu, D.A.–A. Rodriguez*, "Stationary flow of blood in a rigid vessel in the presence of an external magnetic field: considerations about the forces and wall shear stresses", Applied Mathematics, **vol. 7**, pp. 130–136, 2016.
[5]. *I. Hoke, C. Dahmani, T. Weyh*, "Design of a high field gradient electromagnet for magnetic drug delivery to a mouse brain", *Proceedings of the COMSOL Conference*, 2008, Hannover.
[6]. ***LexInnova, "Nanoparticles smart drug delivery system for cancer", http://www.wipo.int/edocs/plrdocs/en/lexinnova_nanoparticles_smart_delivery_system_for_tumors.pdf
[7]. *R. Thomas, I.–K. Park, YY. Jeong*, "Magnetic iron oxide nanoparticles for multimodal imaging and therapy of cancer" Int. J. Mol. Sci. 2013 Jul 31; **vol. 14**, no. 8, pp. 15910–15930, DOI: 10.3390/ijms140815910.
[8]. *A.M. Morega, A.A. Dobre, M. Morega, A. Săndoiu*, "Constructal optimization of magnetic field source in magnetic drug targeting therapy", Proc. Ro. Acad., Series A, **vol. 19**, Special Issue, pp. 123–128, Bucharest, 2018.
[9]. *C.I. Mocanu*, Bases of Electrotechnics – The Theory of Electromagnetic Field (in Romanian), Ed. II, Editura Didactică şi Pedagogică, Bucureşti, ISBN 973-30-1097-9.
[10]. *W.Quanyu, L. Xiaojie, P. Lingjiao, T. Weige, Q. Chunqi,* "Simulation analysis of blood flow arteries of the human arm", Biomedical engineering : applications, basis, and communications, 2017; **vol. 29**, 4, art. no. 1750031.
[11]. ***Comsol Multiphysics, v.3.5a,…5.3a.
[12]. Ningbo Tongchuang Strong Magnet Material Co., Ltd, https://tcmagnet.en.made-in-china.com/
[13]. *J. Pyrhönen; T. Jokinen; V. Hrabovcová*, Design of Rotating Electrical Machines, Wiley, 2009, cited by https://en.wikipedia.org/wiki/Neodymium_magnet